Topological solitons in liquid crystals

Kuan-Sen Lin[1, *]

[1] *Department of Physics, University of Illinois at Urbana-Champaign*

Abstract. Ordered media such as liquid crystals (LCs) provide a platform to realize and manipulate nontrivial field configurations in which topological solitons can emerge and behave like particles. In this term essay, we describe some of the most recent studies on numerical modeling, experimental observation, and manipulation of various topological solitons, such as hopfions, skyrmions, and heliknotons, in LCs. In particular, such topological solitons can be tuned electrically, and interact to form emergent structures, such as skyrmion bags and three-dimensional crystals.

CONTENTS

I. INTRODUCTION

Topological solitons are continuous and localized field configurations that can not be continuously deformed into a trivial, such as a uniform, configuration[1]. Such nontrivial field configurations can behave like particles, and people have been fascinated by this idea for a long time. For example, Gauss proposed that knots in fields could behave like particles[2], and Kelvin suggested that atoms could be represented by knotted structures in an ideal fluid[3]. Liquid crystal (LC), as a reconfigurable and electrically tunable ordered matter, provides a facile platform to create and manipulate topological solitons. In this term essay, we will review the most recent progress in understanding solitons in LCs, including their internal nontrivial structure, their response to external stimuli, pair interactions between solitons, and emergent solitonic condensed matter[2,4,5]. This term essay aims to give a broad picture on this currently very active and exciting research field. For rigorous mathematical formulation, numerical and experimental details, we will refer the readers to the cited articles.

II. HOMOTOPY THEORY

In this section, we give a brief introduction to homotopy theory which will allow us to classify topological defects and topological solitons. We will explain the notation $\pi_n(R)$ and, at least in this essay, we wish to distinguish the terms *topological defects* and *topological solitons*[1], as both objects will present in the later experimental observations in LCs.

A. What is an order parameter field n(r)?

We start with the description of the order parameter field $\mathbf{n(r)}$. $\mathbf{n(r)}$ means that at each point $\mathbf{r}$ in the *base space*, we assign an order parameter value $\mathbf{n}$ in the *target space*. $\mathbf{n}$ can be a scalar, vector, tensor or even a direct product of vector and tensor, depending on details of the system. For example, in a two-dimensional (2D) ordinary spin system[6] we will have $\mathbf{r} \in \mathbb{R}^2$, which is the 2D Euclidean plane, and $\mathbf{n} \in S^2$ which characterizes a unit vector in 3D. Therefore, $\mathbf{n(r)}$ can be viewed as a map from the base space to the target space.

B. Homotopy group $\pi_n(R)$

We now introduce the concept of homotopy group $\pi_n(R)$, which classifies different classes of mapping from the *nth-sphere* to the *target space R*. The nth-sphere, S^n, can be thought of as a unit sphere embedded in the $(n+1)$D Euclidean space satisfying $x_1^2+x_2^2+\cdots+x_n^2+x_{n+1}^2 = 1$. This can be understood through one simple example. Consider the case where both the base space and target space are S^1, namely a unit circle. In this case we will be considering $\pi_1(S^1)$. Homotopy theory[6] tells us that $\pi_1(S^1) = \mathbb{Z}$, which means that the mapping $S^1 \to S^1$ can be classified by an integer $\mathbb{Z}$, which will be used for topological defects later.

C. Topological defects and topological solitons

Although the definition of terms can vary in different literature, here we wish to distinguish *topological defects* and *topological solitons*. Let us begin with topological defects. Given a $\mathbf{n(r)}$, wherever in some region of $\mathbf{r}$ the order parameter is not well-defined, we say that
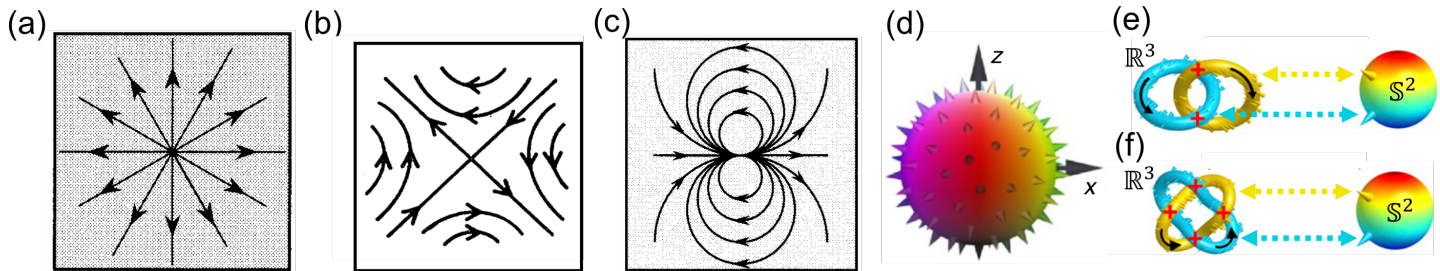
FIG. 1. Examples of homotopy theory. [(a)–(c)] Examples of $S^1 \to S^1$ mapping with winding number $w = 1$, -1 and 2. The arrows can be understood as spins. (d) Example of $S^2 \to S^2$ mapping where the unit vectors denoted as cones cover the entire S^2 once. [(e) and (f)] Closed loop preimages in $\mathbb{R}^3$ (left) of two distinct $\mathbf{n} \in S^2$ marked as yellow and blue cone (right) where the preimages linked (e) once and (f) twice. Figures are taken from Refs. [4–7].

there are defects in that region[1]. A topological defect is a $\mathbf{n}(\mathbf{r})$ configuration with defects that can not be continuously deformed into a uniform configuration. For example, consider a 2D spin system whose spins can only point along the 2D plane, see Fig. 1(a). At the origin of Fig. 1(a), $\mathbf{n}(\mathbf{r})$ is not well-defined. And we can classify this defect by considering a closed S^1 loop $\mathcal{C}$ enclosing the origin. Along $\mathcal{C}$, $\mathbf{n}(\mathbf{r})$ is well-defined, which realizes a mapping from S^1 to S^1, which is classified by $\mathbb{Z}$, see Sec. II B. Physically, this can be understood as how many times, called w, the spin rotates along $\mathcal{C}$ by an angle 2π. Figs. 1(a)–1(c) show configurations of topological point defects with $w = 1$, -1 and 2.

Next, let us consider topological solitons, which is a continuous $\mathbf{n}(\mathbf{r})$ that is well-defined at *every point of the base space* but nevertheless can not be continuously deformed into a uniform $\mathbf{n}(\mathbf{r})$. For example, consider the case where both the base space and target space are S^2. Homotopy theory[6] tells us that $\pi_2(S^2) = \mathbb{Z}$. This means that such a continuous $\mathbf{n}(\mathbf{r})$ is classified by an integer $\mathbb{Z}$. In this case, this can be understood as how many times the unit vectors of $\mathbf{n}(\mathbf{r})$ for all $\mathbf{r}$ cover the entire S^2. For example, Fig. 1(d) shows a $\mathbf{n}(\mathbf{r})$ covering the entire S^2 once, and so this topological soliton has topological number 1.

III.   CHIRAL LIQUID CRYSTAL

In this section we will describe the $\mathbf{n}(\mathbf{r})$ of LC, its free energy functional and the current experimental techniques to obtain high-resolution images of LC's $\mathbf{n}(\mathbf{r})$.

A.   Order parameter

LC is an ordered fluid with either long-range, partial, or no orientational order[8], and can be composed of small molecular rods whose order parameter field, also known as the *director field*, can be represented as $\mathbf{n}(\mathbf{r})$, where $\mathbf{r} \in \mathbb{R}^3$ is our physical 3D space and $\mathbf{n}$ is a nonpolar unit vector with head-tail symmetry such that $\mathbf{n} \equiv -\mathbf{n}$. We then say that $\mathbf{n} \in S^2/\mathbb{Z}_2$ (see Ref. [4]) *which means that we identify the antipodal points on the S^2.* Therefore, we have that a 3D liquid crystal director field $\mathbf{n}(\mathbf{r})$ has $\mathbf{r} \in \mathbb{R}^3$ and $\mathbf{n} \in S^2/\mathbb{Z}_2$. Practically, to facilitate the discussion of solitons and visualize the LC's director field, one will consistently decorate the director field by a unit vector field such that we have $\mathbf{n} \in$

S^2. The mathematical reason[5] is that in a simply connected manifold, for example $\mathbb{R}^3$, a smooth director field with $\mathbf{n} \equiv -\mathbf{n}$ can always be *vectorized* into a *smooth unit vector field* $\mathbf{n}(\mathbf{r}) \in S^2$. This is a process where we change the target space from $S^2/\mathbb{Z}_2$ to S^2. Therefore we will vectorize the director field $\mathbf{n}(\mathbf{r})$ such that $\mathbf{r} \in \mathbb{R}^3$ and $\mathbf{n} \in S^2$ in below.

B. Frank–Oseen free-energy functional

With $\mathbf{n}(\mathbf{r}) \in S^2$, the Frank–Oseen free-energy functional of a 3D *chiral* LC is given by[2,4,5]

$$F[\mathbf{n}(\mathbf{r})] = \int d^3\mathbf{r} \left(\frac{K}{2}(\nabla \mathbf{n})^2 + \frac{2\pi K}{p} \mathbf{n} \cdot (\nabla \times \mathbf{n}) - \frac{\varepsilon_0 \Delta \varepsilon}{2}(\mathbf{n} \cdot \mathbf{E})^2 \right), \tag{1}$$

where K is the elastic constant, $\Delta \varepsilon$ is the LC's dielectric anisotropy, $\mathbf{E}$ is the external electric field. The local minima of $F[\mathbf{n}(\mathbf{r})]$ represent $\mathbf{n}(\mathbf{r})$ that might be observed experimentally. The first and third term in Eq. (1) represent the elastic deformation energy and the coupling between LC and $\mathbf{E}$. When $\Delta \varepsilon > 0$ $[\Delta \varepsilon < 0]$, the LC molecules will tend to be parallel [perpendicular] to $\mathbf{E}$. The second term is the *chiral* term, whose effect is to make the LC molecules twist along a *helical axis* $\boldsymbol{\chi}$, and p is the distance over which the LC molecules twist 2π angle. Experimentally, such a twisting can be induced by adding chiral dopant into the LC[4]. For example, in Fig. 6(a) we show such a twisting of $\mathbf{n}(\mathbf{r}) \in S^2$ (left) and the actual LC molecule (right) twisting, both along the helical axis $\boldsymbol{\chi}$. The key message from this $F[\mathbf{n}(\mathbf{r})]$ is that the competition between the external field, elastic deformation and chirality can lead to a plethora of nontrivial field configurations.

C. Nonlinear optical imaging technique

Before we delve into the experimental studies of solitons in chiral LCs, let us describe how people can obtain high-resolution image of the $\mathbf{n}(\mathbf{r})$. This is done through three-photon excitation fluorescence polarizing microscopy[4] (3PEF-PM). The simplified working principle is as follow. A polarized light will be used to excite the LC molecules through a three-photon process, which means that there will be three photons absorbed by a LC molecule. The excited LC molecules will then emit fluorescence light. We then detect the intensity of such fluorescence light. Crucially, the intensity scales as $\cos^6 \beta$ where β is the angle between the polarization of the light and the direction of $\mathbf{n}(\mathbf{r})$. Therefore, by using different polarized lights and scan through the sample, we can reconstruct the LC's $\mathbf{n}(\mathbf{r})$.

IV. ELECTRICALLY TUNABLE HOPFION

Let us delve into the first topological soliton in this term essay – *hopfion*. We will describe the creation and manipulation of hopfions in chiral LCs. In particular, the topological structure of the soliton can be tuned by applied electric fields[4], as we will describe below.

A. The concept of far-field and preimage

To obtain the topological classification of hopfion using homotopy theory, we assume that the director field $\mathbf{n}(\mathbf{r})$ at the *boundary* of the 3D sample points along the same direction

$\mathbf{n}_0$, which is called the *far-field*. In such a case, we can perform a compactification[4] to map the $\mathbf{r}$ in $\mathbf{n}(\mathbf{r})$ from $\mathbb{R}^3$ to S^3. Therefore our base space becomes S^3, and then we can apply homotopy theory. The relevant homotopy groups are $\pi_3(S^2) = \pi_3(S^2/\mathbb{Z}_2) = \mathbb{Z}$ (see Ref. [4]), where recall that the LC has its target space $S^2/\mathbb{Z}_2$ and then we vectorize it to be S^2. Therefore, given a fixed far-field $\mathbf{n}_0$, solitons in chiral LCs are classified by an integer $\mathbb{Z}$. Let us call this integer Q. This Q is also called the *Hopf index*[4]. In fact, given a unit vector field $\mathbf{n}(\mathbf{r})$ with fixed far-field $\mathbf{n}_0$ we can compute Q through[4]

$$Q = \frac{1}{64\pi^2} \int_{\mathbb{R}^3} d^3\mathbf{r}\,\epsilon^{ijk} A_i F_{jk}, \tag{2}$$

where $F_{ij} = \mathbf{n} \cdot (\partial_i \mathbf{n} \times \partial_j \mathbf{n})$, and A_i is defined through $F_{ij} = (\partial_i A_j - \partial_j A_i)/2$ which can be computed numerically given the vectorized director field $\mathbf{n}(\mathbf{r})$.

To understand the topological significance of a $\mathbf{n}(\mathbf{r})$ with nonzero Q, let us introduce the concept of *preimage*. Given a $\mathbf{n}(\mathbf{r})$, the preimage of a constant $\mathbf{n}_1 \in S^2$ is a region in the base space where $\mathbf{n}(\mathbf{r}) = \mathbf{n}_1$. In particular for the mapping $S^3 \to S^2$, the preimage of a $\mathbf{n}_1 \in S^2$ will be a collection of closed loops in S^3, or $\mathbb{R}^3$ with a fixed far-field[8]. With the concept of preimage, there is a simple way that we can visualize a $\mathbf{n}(\mathbf{r})$ with $Q \neq 0$. When $Q \neq 0$, the preimages of *any two distinct* $\mathbf{n} \in S^2$ will be closed loops that link with each other Q times. As a demonstration, in Fig. 1(e) [1(f)] we show the preimages of two *distinct* points on S^2 for $\mathbf{n}(\mathbf{r})$ with $Q = 1$ [$Q = 2$]. As we can see the closed loop preimages in Fig. 1(e) [1(f)] link with each other once [twice]. The key message here is that a $Q \neq 0$ hopfion has preimages of *any* two distinct $\mathbf{n} \in S^2$ be closed loops linked Q times.

B. Tuning the internal structure of hopfions using electric field

Having understood the concept of preimage and how to determine Q by counting the linking number of closed loop preimages, we now demonstrate how the hopfion's internal structure can be tuned[4] by an applied voltage U along the far-field direction $\mathbf{n}_0 = (0, 0, 1)$, namely we apply an electric field $\mathbf{E} \parallel \mathbf{n}_0$. In this section, the chiral LCs have $\Delta\varepsilon < 0$.

When $U = 0$, the researchers first realize a $Q = -2$ micrometer-sized hopfion, whose simulated $\mathbf{n}(\mathbf{r})$ is shown in Fig. 2(a), and the preimages of two distinct $\mathbf{n} \in S^2$ form a pair of Hopf link, each with $Q = -1$, and so the total $Q = -2$, as shown in Fig. 2(d). When U is increased to $2.6\text{V} < U < 4.2\text{V}$, the researchers found that a *boundary line* at polar angle θ_c measured from the north pole appears in the target space S^2. For a $\mathbf{n}$ with $\theta < \theta_c$ [$\theta > \theta_c$], its preimage is composed of a single closed loop [two separated closed loops]. Importantly, when $2.6\text{V} < U < 4.2\text{V}$, the Q of $\mathbf{n}(\mathbf{r})$ is still -2. For example, the simulated $\mathbf{n}(\mathbf{r})$ for $U = 3.6\text{V}$ is shown in Fig. 2(b), where the researchers confirm numerically that this $\mathbf{n}(\mathbf{r})$ carries $Q = -2$. Therefore, when $U = 3.6\text{V}$, suppose we choose two distinct $\mathbf{n}_1$ and $\mathbf{n}_2$ on S^2, there exist different ways that their preimages link to give $Q = -2$. In particular, there will be three cases: (1) both $\mathbf{n}_1$ and $\mathbf{n}_2$ have $\theta < \theta_c$, (2) one of $\mathbf{n}_1$ and $\mathbf{n}_2$ has $\theta < \theta_c$ and the other has $\theta > \theta_c$, (3) both $\mathbf{n}_1$ and $\mathbf{n}_2$ have $\theta > \theta_c$. These three cases (all have $Q = -2$) are shown in Figs. 2(g), 2(f), 2(e), respectively. Finally, when $U > 4.2\text{V}$, the Q of $\mathbf{n}(\mathbf{r})$ changes from $Q = -2$ to $Q = -1$, where the simulated $\mathbf{n}(\mathbf{r})$, and the preimages of two distinct $\mathbf{n} \in S^2$ linked once are shown in Figs. 2(c) and 2(h), respectively. Furthermore, the researchers obtain a relation between θ_c, Q and U, which is shown in Fig. 2(i). As we can see, when $U < 2.6\text{V}$, the hopfion has $Q = -2$ and the preimages of any two distinct

$\mathbf{n} \in S^2$ form a pair of Hopf links. When $U = 2.6$V, there is a abrupt appearance of a nonzero $\theta_c = 68°$ and when 2.6V $< U < 4.2$V, there exist three different types of linked preimages, all giving $Q = -2$. The θ_c will slightly increase as we increase U, but then when $U = 4.2$V, the hopfion undergoes a topological transformation from $Q = -2$ to $Q = -1$ and there will be no θ_c hereafter.
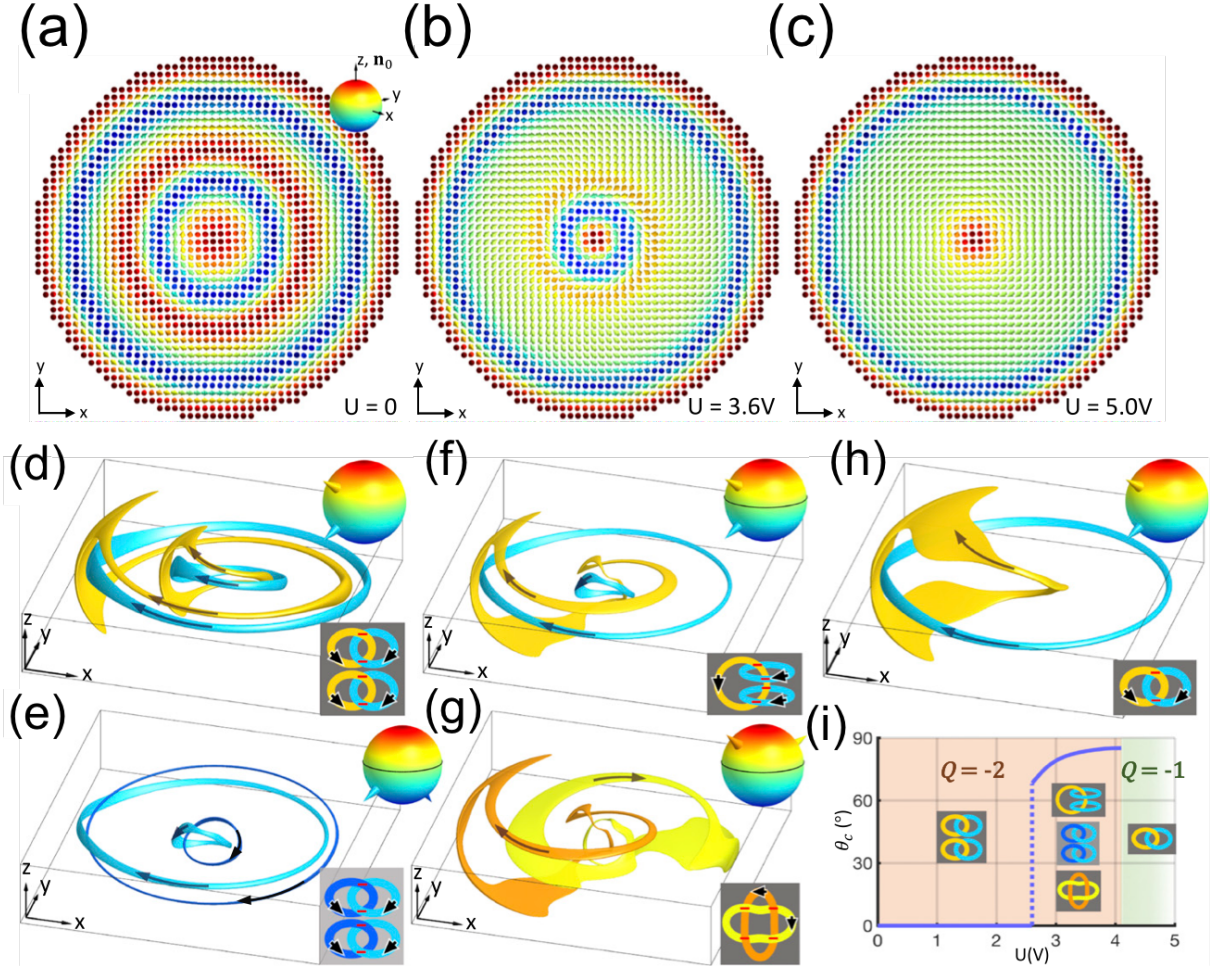
FIG. 2. Electrically tunable hopfions. [(a)–(c)] Top view of the simulated $\mathbf{n}(\mathbf{r})$ at the midplane cross-section of a 3D chiral LC sample at applied voltage $U = 0$, 3.6 and 5.0V. [(d)–(g)] The closed loop preimages in $\mathbb{R}^3$ of points on S^2 indicated as cones in the *upper right insets*. The *lower right insets* of (d)–(g) are the schematics of the linking of preimages. (d) and (h) correspond to the hopfions shown in (a) and (c) where the closed loop preimages linked twice and once. (f), (e) and (g) correspond to three different types of closed loop preimages linked twice at $U = 3.6$V in (b). The boundary line with polar angle θ_c is indicated as the black line in the *upper right insets* of (f), (e) and (g). (i) The relation between θ_c, Q and U. Figures are taken from Ref. [4].

What we have described above are all simulation results. Importantly, all of them are confirmed by experiment. Shown in Figs. 3(a)–3(f) are the experimental and simulation results of nonlinear optical imaging, described in Sec. III C. Figs. 3(a) and 3(d) correspond to Fig. 2(a) imaged using polarized light along the horizontal and vertical directions, respectively. Similarly, Figs. 3(b) and 3(e) [3(c) and 3(f)] correspond to Fig. 2(b)

[2(c)]. As we can see the experiment and simulation match with each other, meaning that hopfions in chiral LC can be tuned electrically and undergo topological transformation[4].
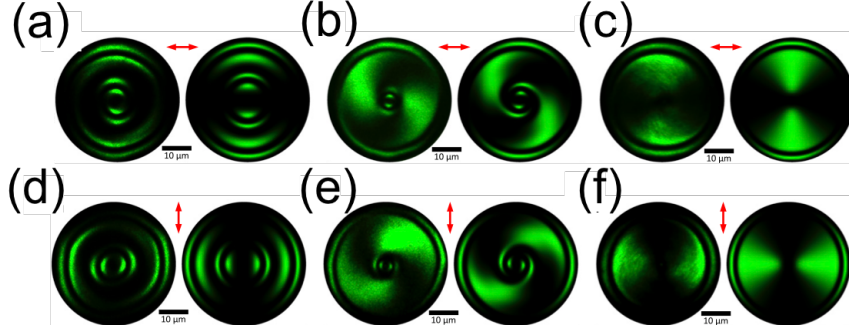
FIG. 3. [(a)–(f)] Midplane cross-sectional nonlinear optical images (left) and computer-simulated optical images (right) of hopfions in Fig. 2(a)[(a)&(d)], Fig. 2(b)[(b)&(e)] and Fig. 2(c)[(c)&(f)]. The polarization of lights are marked as double arrows at the top of the images. Regions with bright green color have $\mathbf{n(r)}$ closely aligned to the polarization. Figures are taken from Ref. [4].

V. SKYRMION BAG

In this section, we describe the creation of stable, particle-like *skyrmion bag* with *arbitrary* topological degree Q in chiral LCs[5]. This can potentially apply to display technology where we store a large amount of information that is stable both energetically and topologically.

A. The topological degree Q

We begin with the classification of nontrivial $\mathbf{n(r)}$. We will consider a 3D chiral LC but assume that $\mathbf{n(r)}$ is constant along the z direction. Therefore, the effective base space, with fixed far-field $\mathbf{n}_0$, is S^2. The relevant homotopy groups are then $\pi_2(S^2) = \pi_2(S^2/\mathbb{Z}_2) = \mathbb{Z}$ (see Refs. [6 and 8]). We will call this $\mathbb{Z}$ integer invariant the topological degree Q, which can be computed using[5]

$$Q = \frac{1}{4\pi} \int_{\mathbb{R}^2} d^2\mathbf{r} \left[\mathbf{n} \cdot (\partial_x \mathbf{n} \times \partial_y \mathbf{n})\right]. \tag{3}$$

Pictorially, Q corresponds to how many times the S^2 target space is covered by $\mathbf{n(r)}$ for all $\mathbf{r} \in \mathbb{R}^2$. Shown in Fig. 4(a) is a skyrmion tube translationally invariant along z with $Q = -1$. The color of $\mathbf{n(r)}$ is drawn according to Fig. 4(b). The top view of Fig. 4(a) is shown in Fig. 4(c) where we can see that at the origin of the disk the $\mathbf{n}$ points along $(0,0,-1)$ while as we approach the boundary, $\mathbf{n}$ gradually twists to point along $(0,0,1)$. In this case, all the $\mathbf{n}$ shown in Fig. 4(c) will cover S^2 once. And the $\mathbf{n(r)}$ in Fig. 4(c) will be called a *full skyrmion*, where we introduce a π-twist in $\mathbf{n(r)}$ from the origin to the boundary. We can add a further π-twist in Fig. 4(c) to obtain Fig. 4(d) where as we go from the origin to the boundary, the $\mathbf{n}$ changes from $(0,0,1)$, to $(0,0,-1)$, and finally back to $(0,0,1)$. However, in this case, $Q = 0$. This means that we can perform a continuous deformation such that we change Fig. 4(d) to a uniform configuration, see the Supplementary Video 2 of Ref. [5].
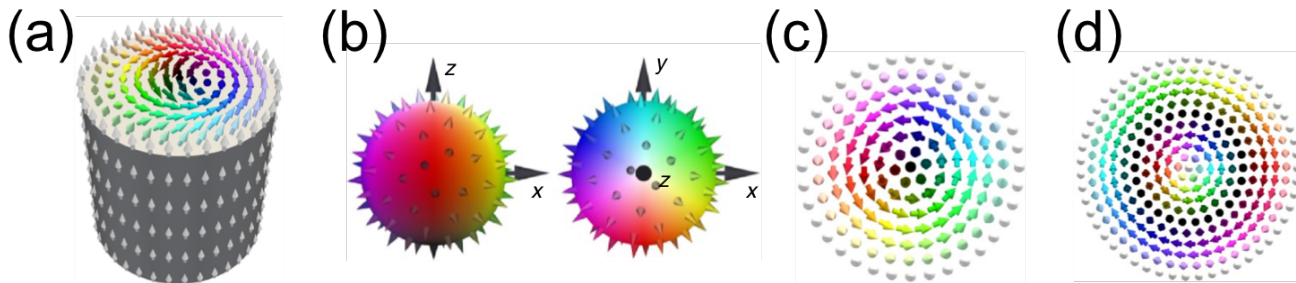
FIG. 4. (a) A translationally invariant skyrmion tube with colored $\mathbf{n}(\mathbf{r})$ according to their directions on the S^2 in (b). (b) The colored sphere is used for dressing $\mathbf{n}(\mathbf{r})$ in (a), (c) and (d). (c) corresponds to a full skyrmion with $Q = -1$. (d) corresponds to a $\mathbf{n}(\mathbf{r})$ with $Q = 0$. Figures are from Ref. [5].

B. Particle behavior of full skyrmions

Full skyrmions can behave like particles. For example, they can move around in the chiral LC and interact with each other. Using $F[\mathbf{n}(\mathbf{r})]$ in Eq. (1), it can be shown the the pair potential between two full skyrmions is repulsive and has the asymptotic form[5]

$$V_{\text{int}}(R) = a\frac{e^{-bR}}{\sqrt{R}}, \tag{4}$$

where a and b are positive constants related to the materials parameter, and R is the distance between the two full skyrmions. Shown in Fig. 5(a) is the experimentally measured repulsive force between two full skyrmions, and the inset is the optical image of the two full micrometer-sized skyrmions. The blue points are experimental data and the orange line is the fitted curve to the asymptotic pair potential (4), which show great agreement.

The next question is whether we can create a long-lived structure of $\mathbf{n}(\mathbf{r})$ with $|Q| > 1$. This is a nontrivial question, as quoted from Ref. [5] *only fractional and full skyrmions have previously been realized in chiral condensed-matter systems* by the time Ref. [5] is published.

C. Long-lived skyrmion bag with arbitrary Q

In this work, a long-lived *skyrmion bag* is created by putting a large amount of anti-skyrmions, each with $Q = +1$, inside a stretched skyrmion with $Q = -1$, which serve as the outer bag. Suppose we place N_A antiskyrmions inside one skyrmion bag, we can realize a $\mathbf{n}(\mathbf{r})$ with $Q = N_A - 1$. We will then denote such a skyrmion bag as $S(N_A)$. Shown in Fig. 5(b) from left to right are $S(1)$–$S(4)$, two types of $S(13)$, and $S(59)$. Surprisingly, for $S(N_A)$ bag with $N_A > 1$, they can stay topologically unchanged for *more than one year already* by the time Ref. [5] is published. And as N_A increases, $S(N_A)$ becomes more stable[5].

One of the reason for the stability as N_A increases is that, as we can see in the case of $S(59)$, the antiskyrmions inside the bag self-organize to form a 2D hexagonal lattice such that it is energetically unfavorable to slightly deviate one antiskyrmion from its equilibrium position. Furthermore, a natural inter-skyrmion distance has emerged[5]. Therefore, the stability may be understood as a result of emergent lattice structure with its rigidity.

Being stable, we can then ask whether $S(N_A)$ behaves like a particle. This can be verified by measuring the repulsive force between two $S(3)$, which is shown in Fig. 5(c). As
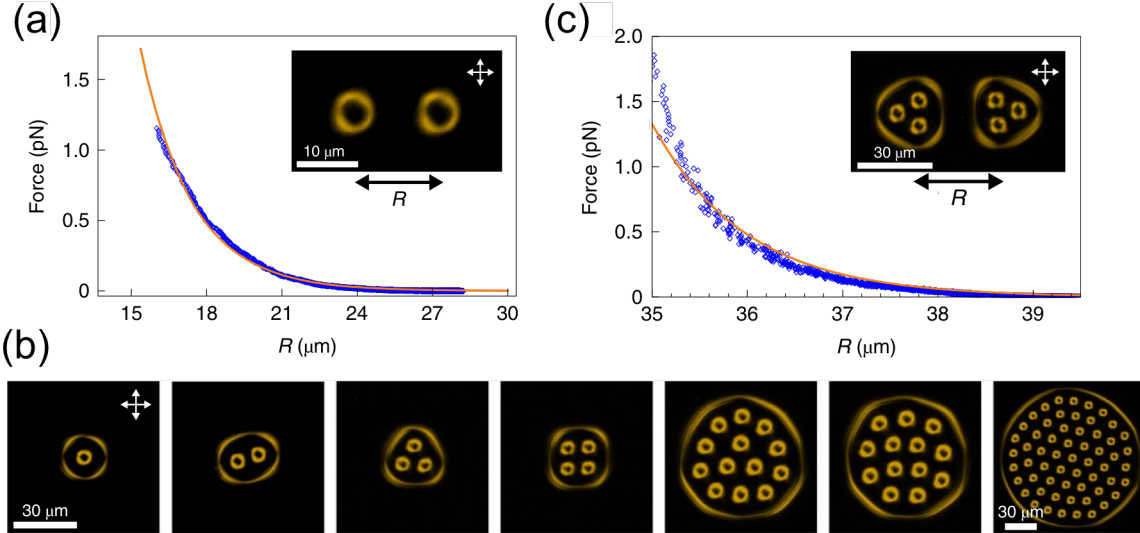
FIG. 5. [(a) and (c)] Experimentally measured force (blue points) and the fitted orange curve to the asymptotic pair potential (4) between two (a) full skyrmions and (b) S(3) bags, where the upper right insets correspond to their optical images. (b) Optical images of S(1)–S(4), two types of S(13) and S(59) bags from left to right. Figures are taken from Ref. [5].

we can see, the experimentally measured force between the two $S(3)$ bags fitted nicely to the asymptotic $V_{\text{int}}(R)$ in Eq. (4). Therefore $\boxed{S(N_A) \text{ bags indeed behave like particles.}}$

VI. SELF-ASSEMBLED CRYSTAL OF HELIKNOTON

In this section, we consider another soliton that can appear in chiral LCs – *heliknoton*. We will demonstrate that they can behave like particles, and can self-organize into various hierarchical 2D and 3D lattice structures[2]. The chiral LCs considered here have $\Delta\varepsilon > 0$.

A. Helical field

As we mentioned before, the second term in the free energy functional (1) introduces a twisting tendency of LC molecules along the so-called helical axis $\boldsymbol{\chi}$. When such twisting is not frustrated, we can attach a triad of orthonormal fields at each point of the chiral LC, which we will call $\mathbf{n}(\mathbf{r})$, $\boldsymbol{\chi}(\mathbf{r})$ and $\boldsymbol{\tau}(\mathbf{r})$. $\mathbf{n}(\mathbf{r})$ is the vectorized director field of LC. $\boldsymbol{\chi}(\mathbf{r})$ is a nonpolar field along the helical axis. And $\boldsymbol{\tau}(\mathbf{r}) = \mathbf{n}(\mathbf{r}) \times \boldsymbol{\chi}(\mathbf{r})^2$ is also a nonpolar field. In Fig. 6(a) we show a helical field with $\mathbf{n}(\mathbf{r})$, $\boldsymbol{\chi}(\mathbf{r})$ and $\boldsymbol{\tau}(\mathbf{r})$ where $\mathbf{n}(\mathbf{r})$ is either polar or nonpolar. Recall that when we say $\mathbf{n}$ is nonpolar we mean that $\mathbf{n} \equiv -\mathbf{n}$ such that $\mathbf{n} \in S^2/\mathbb{Z}_2$. Notice that both $\boldsymbol{\chi}(\mathbf{r})$ and $\boldsymbol{\tau}(\mathbf{r})$ are immaterial and nonpolar fields.

B. Heliknoton: topological classification

Given a helical far-field background with fixed helical axis $\boldsymbol{\chi}_0$, a new type of soliton, *heliknoton*, can emerge. First, the $\mathbf{n}(\mathbf{r})$ will again be continuous and classified by the Hopf index[2] Q since $\pi_3(S^2) = \pi_3(S^2/\mathbb{Z}_2) = \mathbb{Z}$ as in Sec. IV A. In addition, there can exist *topological line defects* in the nonpolar $\boldsymbol{\chi}(\mathbf{r})$ and $\boldsymbol{\tau}(\mathbf{r})$. In a 3D system with nonpolar field, we
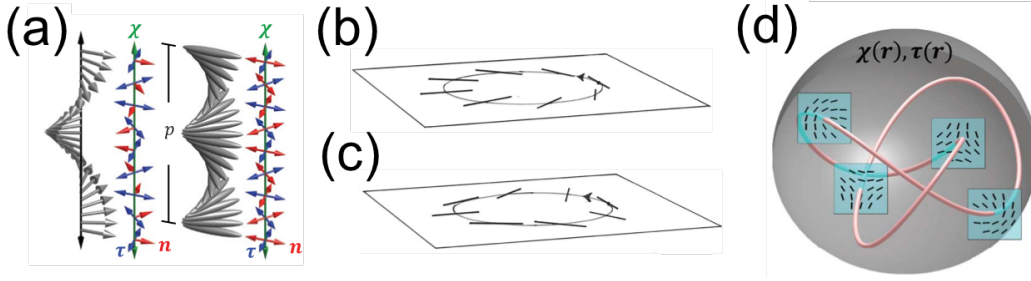
FIG. 6. (a) Helical field composed of a triad of orthonormal fields $\mathbf{n}(\mathbf{r})$, $\boldsymbol{\chi}(\mathbf{r})$ and $\boldsymbol{\tau}(\mathbf{r})$ where $\mathbf{n}(\mathbf{r})$ is either polar (left) or nonpolar (right). The helical pitch p is also indicated. [(b) and (c)] Two topologically equivalent examples of the orientation of nonpolar fields around a vortex line. (d) Colocated self-knotted vortex lines in $\boldsymbol{\chi}(\mathbf{r})$ and $\boldsymbol{\tau}(\mathbf{r})$ where the cross-sections show schematic orientations of $\boldsymbol{\chi}(\mathbf{r})$ and $\boldsymbol{\tau}(\mathbf{r})$ around the vortex line. Figures are taken from Refs. [2 and 9].

can have line defects classified by the first homotopy group[6,9] $\pi_1(S^2/\mathbb{Z}_2) = \mathbb{Z}_2$. Shown in Figs. 6(b) and 6(c) are two topologically equivalent topological line defects[9] for a nonpolar field. We can see that the nonpolar field rotates $\pm 180°$ when we go around a closed loop enclosing the *line defect*, at which the direction of nonpolar fields is not well-defined. For this reason, we will call such line defects as *vortex lines* hereafter. Since $\boldsymbol{\tau}(\mathbf{r})$ is derived from $\boldsymbol{\chi}(\mathbf{r})$, $\boldsymbol{\chi}(\mathbf{r})$ and $\boldsymbol{\tau}(\mathbf{r})$ *share the same vortex line.* Such a vortex line can be self-knotted, see Fig. 6(d). Crucially, if $\boldsymbol{\chi}(\mathbf{r})$ and $\boldsymbol{\tau}(\mathbf{r})$ are polar and belong to S^2 instead of $S^2/\mathbb{Z}_2$, then $\pi_1(S^2) = 0$ means there is no topological line defect[6]. It is precisely the *nonpolar* nature of $\boldsymbol{\chi}(\mathbf{r})$ and $\boldsymbol{\tau}(\mathbf{r})$ that allows the existence of topological line defects, as $\pi_1(S^2/\mathbb{Z}_2) = \mathbb{Z}_2$. Therefore, heliknoton[2] in *helical* fields is a *soliton* composed of linked preimages in $\mathbf{n}(\mathbf{r})$ and *knotted* vortex lines in $\boldsymbol{\chi}(\mathbf{r})$ and $\boldsymbol{\tau}(\mathbf{r})$[10]. We will see the visualization in the next section.

C. Heliknoton: examples of $Q = 1$ and $Q = 2$ and experimental images

Shown in Figs. 7(a)–7(c) [7(d)–7(f)] are the simulated $\mathbf{n}(\mathbf{r})$, $\boldsymbol{\chi}(\mathbf{r})$ and $\boldsymbol{\tau}(\mathbf{r})$ for $Q = 1$ [$Q = 2$] heliknoton. In particular, in Fig. 7(a) [7(d)] the preimages of the north and south pole of S^2 are plotted as white and black closed loops that link once [twice], which means $Q = 1$ [$Q = 2$], and schematic figures of the preimage are shown in the upper right insets. Furthermore, in Figs. 7(b) and 7(c) [7(e) and 7(f)] the vortex lines are shown as self-knotted pink tubes and can be deformed into the configurations shown in the upper right insets, and from the top view these self-knotted vortex lines have crossing number $N = 3$ [$N = 5$]. In fact, there is a relation between Q and N, which is $N = 2Q + 1$ (see Ref. [2]).

Shown in Fig. 7(g) is the optical image of coexisting micrometer-sized $Q = 1$ (left) and $Q = 2$ (right) heliknotons in a LC with thickness $d = 20\mu m$ when the applied voltage is $U = 2.0$V along the far-field $\boldsymbol{\chi}_0$ and they can be schematically denoted as the cartoon figures in Figs. 7(h) and 7(i), where the black and white closed loops are the preimages of the north and south pole of S^2 and the pink tubes are the self-knotted vortex lines in $\boldsymbol{\chi}(\mathbf{r})$ and $\boldsymbol{\tau}(\mathbf{r})$.

As a remark, notice that the heliknoton is a localized field configuration where all of $\mathbf{n}(\mathbf{r})$, $\boldsymbol{\chi}(\mathbf{r})$ and $\boldsymbol{\tau}(\mathbf{r})$ are highly twisted locally, as shown in Figs. 7(a)–7(f). Therefore, heliknoton is a *combination* of linked preimages in $\mathbf{n}(\mathbf{r})$ and self-knotted vortex lines in $\boldsymbol{\chi}(\mathbf{r})$ and $\boldsymbol{\tau}(\mathbf{r})$.
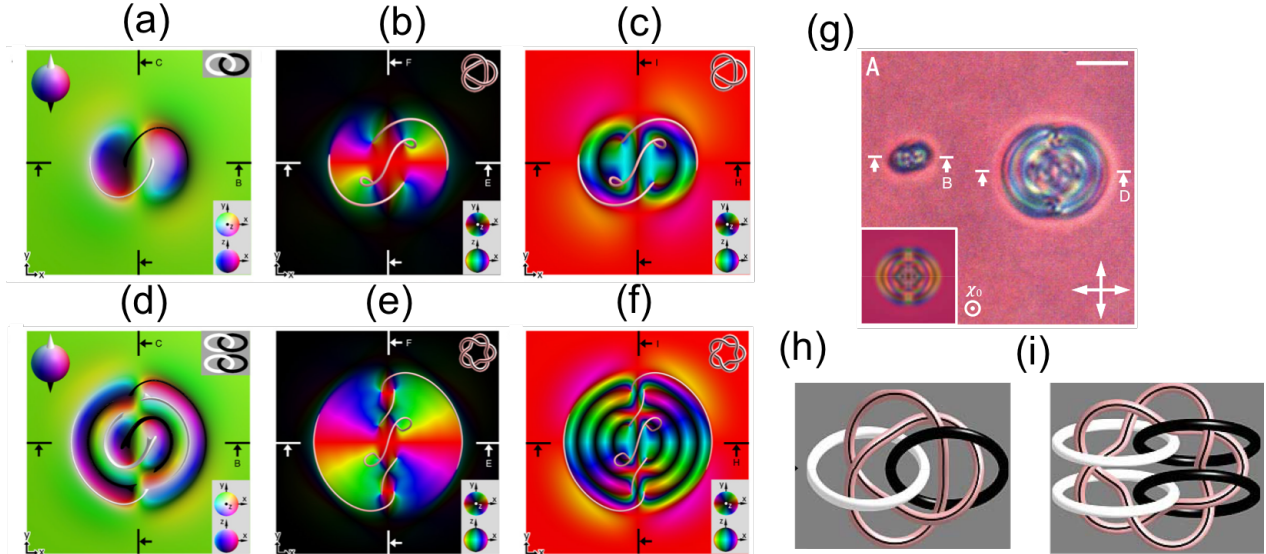
FIG. 7. [(a)–(c)] Computer-simulated midplane cross-section of $\mathbf{n}(\mathbf{r})$, $\boldsymbol{\chi}(\mathbf{r})$ and $\boldsymbol{\tau}(\mathbf{r})$ for a $Q = 1$ heliknoton in a 3D sample. [(d)–(f)] Computer-simulated midplane cross-section of $\mathbf{n}(\mathbf{r})$, $\boldsymbol{\chi}(\mathbf{r})$ and $\boldsymbol{\tau}(\mathbf{r})$ for a $Q = 2$ heliknoton in a 3D sample. The upper right insets of (a) and (d) show schematics of the linked preimages in $\mathbf{n}(\mathbf{r})$ with $Q = 1$ and $Q = 2$, respectively. The upper right insets of (b)–(c) and (e)–(f) show schematics of self-knotted vortex lines with crossing number $N = 3$ and $N = 5$, respectively. (g) Optical images of $Q = 1$ (left) and $Q = 2$ (right) heliknotons. [(h) and (i)] Schematics of linked preimages (black and white loops) in $\mathbf{n}(\mathbf{r})$ and self-knotted vortex lines (pink tubes) in $\boldsymbol{\chi}(\mathbf{r})$ and $\boldsymbol{\tau}(\mathbf{r})$ for (h) $Q = 1$ and (i) $Q = 2$ heliknotons. Figures are taken from Ref. [2].

D. Heliknotons as interacting particles

Given that heliknotons are localized field configurations, we can then ask whether they behave like particles. Fig. 8(a) shows a gas of $Q = 1$ heliknotons. And their pair interaction is highly tunable through different LCs, applied voltage U and the thickness d of the sample, as shown in Fig. 8(b), which is the experimentally measured (attractive) pair potential. In a thick enough LC sample, we can actually see that two $Q = 1$ heliknotons attract each other and form a dimer, as shown in Figs. 8(c) and 8(d) at time $t = 0s$ and $8s$, where the dimer in 8(d) is formed by one heliknoton at top and the other at bottom. Given that it is possible to achieve attractive interactions between heliknotons, the next question is whether they can self-assemble into crystals.

E. Emergent self-assembled two-dimensional crystal

For chiral LC sample with thin enough thickness, such as $d = 10\mu m$, the $Q = 1$ heliknotons with anisometric shape are all located around the horizontal midplane of the sample. The attractive interaction allows heliknotons to self-assemble and form 2D rhombic lattice[2], as shown in Figs. 9(a) and 9(b). We can see that a heliknoton comes in and then is attracted by the already-formed 2D lattice to fill in the groove. With initial positions set by laser tweezers, a stretched kagome lattice[2] can also form, see Fig. 9(c). For a given self-assembled
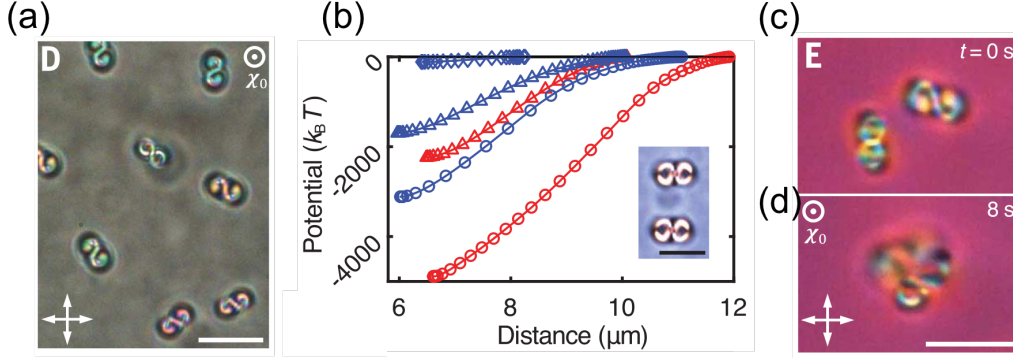
FIG. 8. (a) A gas of heliknotons. (b) The experimentally measured (attractive) pair potentials for different LCs and applied voltage U. [(c) and (d)] Two heliknotons in (c) attract each other and form dimer in (d). Figures are taken from Ref. [2].

crystal structure, the researcher can also change its symmetry by changing U. For example, when we increase U from 1.8V to 2.3V, the orientation of the heliknotons in a 2D lattice can change from synclinic to anticlinic tilting (Figs. 9(d) and 9(e)). In particular, this process is reversible[2]: when U is tuned back to $U = 1.8$V, we can change Fig. 9(e) back to 9(d).
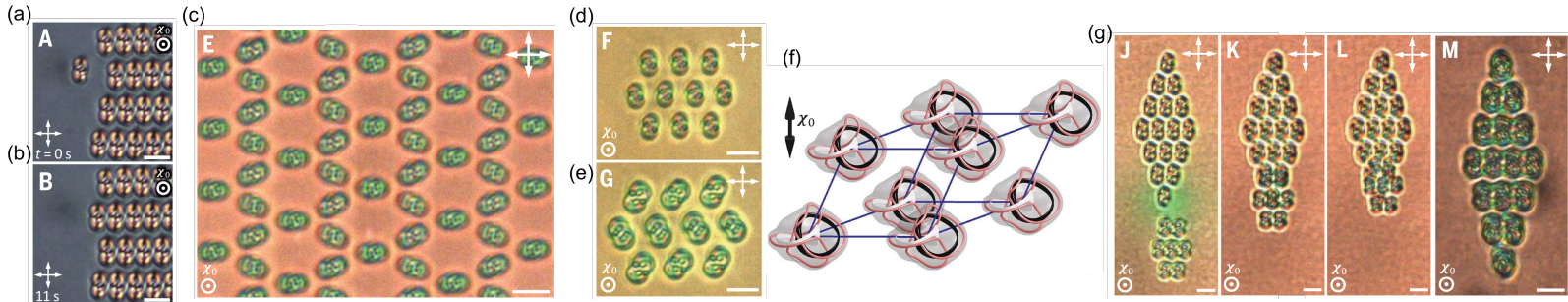
FIG. 9. [(a) and (b)] A heliknoton in (a) is attracted by the 2D crystal and fill in the groove in (b). (c) A 2D stretched kagome lattice formed by heliknotons. [(d) and (e)] 2D lattice with (d) synclinic and (e) anticlinic tilting of heliknotons at $U = 1.8$V and 2.3V, respectively. (f) A schematic figure of a 3D triclinic crystal with heliknotons at its lattice points. (g) From left to right is the process where two 2D heliknoton crystals interact and self-organize into a 3D crystal. Figures are taken from Ref. [2].

F.   Emergent self-assembled three-dimensional crystal

We have seen that a plethora of 2D crystals can emerge in thin enough LC sample. The next question is whether we can realize 3D self-assembled crystals in thick enough LC sample. The answer is excitingly affirmative. Shown in Fig. 9(f) is a schematic figure of a 3D triclinic lattice where the *atoms* at its lattice points are *heliknotons.* To obtain such a 3D crystal, the researchers first form 2D self-assembled rhombic crystal planes, shown in Fig. 9(g), and then these 2D crystal planes interact and move along lateral and axial directions to form a 3D triclinic lattice where one 2D crystal plane is on top of the other.

As a final remark, the experimentally observed heliknoton crystals exist within a broad range of applied voltage U, which really allow us to tune their structures by applying weaker or stronger external electric field $\mathbf{E}$.

VII.   CONCLUSION AND OUTLOOK

In this term essay, we review the most recent progress on various solitons in chiral LCs, including *hopfions*, *skyrmions*, and *heliknotons*. For hopfions, it has been shown that their internal topological structure can be tuned electrically[4]. For skyrmions, researchers have created stable, particle-like skyrmion bag[5] with arbitrary topological degree Q. For helikno-ton, which is a combination of linked preimages and self-knotted vortex lines, it is found that they can self-organize into 2D and 3D crystals whose structures can be tuned electrically[2]. These research works open the door to *solitonic condensed matter*, where soliton is the build-ing block of emergent matter. Although the author of this term essay does not participate in these research works, here are some directions that can possibly be pursued:

1. Effective inertia masses of the solitons

2. The rigidity of the emergent 2D and 3D heliknoton crystals

3. Emergent 2D crystals formed by skyrmion bags $S(N_A)$, where N_A might play the role of *atomic number*, and different N_A can possibly lead to hierarchical structures

4. Critical behavior of solitons when they undergo topological transformation that changes their topological degree Q

The research works described in this term essay will not only provide insights to the under-standing of solitons, but also have potential application to the display technology where we can store information in stable solitons and tune them electrically in chiral LCs.

---

[*] kuansen2@illinois.edu

[1] M. Kleman and O. D. Lavrentovich, eds., "Topological theory of defects," in *Soft Matter Physics: An Introduction* (Springer New York, New York, NY, 2003) pp. 434–471.

[2] J.-S. B. Tai and I. I. Smalyukh, Science **365**, 1449 (2019), https://science.sciencemag.org/content/365/6460/1449.full.pdf.

[3] N. Manton and P. Sutcliffe, *Topological Solitons*, Cambridge Monographs on Mathematical Physics (Cambridge University Press, 2004).

[4] J.-S. B. Tai, P. J. Ackerman, and I. I. Smalyukh, Proceedings of the National Academy of Sciences **115**, 921 (2018), https://www.pnas.org/content/115/5/921.full.pdf.

[5] D. Foster, C. Kind, P. J. Ackerman, J.-S. B. Tai, M. R. Dennis, and I. I. Smalyukh, Nature Physics **15**, 655 (2019).

[6] N. D. Mermin, Rev. Mod. Phys. **51**, 591 (1979).

[7] P. M. Chaikin and T. C. Lubensky, "Topological defects," in *Principles of Condensed Matter Physics* (Cambridge University Press, 1995) p. 495–589.

[8] J.-S. B. Tai, *Topological Solitons in Chiral Condensed Matters*, Ph.D. thesis (2020).

[9] G. P. Alexander, B. G.-g. Chen, E. A. Matsumoto, and R. D. Kamien, Rev. Mod. Phys. **84**, 497 (2012).

[10] Hence the name "heli"+"knot"+"on", since we have a helical-field knot soliton.